RELATÓRIO DE ATIVIDADES

1 – DADOS CADASTRAIS

1.1 Nome do Beneficiário Adriano Peres de Morais	1.2 CPF / Passaporte: 995.103.70-72
1.3 Instituição UNIVERSIDADE FEDERAL DE SANTA MARIA	1.3 Programa CAPES PrInt/ nº do AUXPE CAPES Print- Edital nº 41/2017 Nº **88887.363019/2019-00**
1.5 Projeto RECURSOS ENERGÉTICOS	1.6 Coordenador Projeto Daniel Pinheiro Bernardon.
1.7 Programa de Pós-Graduação PROGRAMA DE PÓS-GRADUAÇÃO EM ENGENHARIA ELÉTRICA	

2 – BENEFÍCIO

2.1 Modalidade: PROFESSOR VISITANTE JÚNIOR ( ) Missão de Trabalho (X) Bolsa 3 x € 2.100,00 (€ 6.300,00)		
2.2 Instituição de Destino Otto-von-Guericke University	2.3 Período da Atividade 2.3.1 Início: 01/10/2019	2.3.2 Término 31/12/2019

3 – RECURSOS RECEBIDOS

3.1 Auxílio-deslocamento	
3.2 Auxílio-instalação	€ 2.100,00
3.3 Seguro-saúde	€ 270,00
3.4 Adicional-localidade	
3.5 Mensalidade	€ 6.300,00 (3 x € 2.100,00)
3.6 Auxílio-diário	

4 – DESCRIÇÃO DAS ATIVIDADES

4.1 Objetivos:

Realização de missão de estudo junto a *Otto-von-Guericke University* na Alemanha, Programa CAPES PrInt pelo Prof. Adriano Peres de Morais, professor permanente do Programa de Pós-Graduação em Engenharia Elétrica – PPGEE da Universidade Federal de Santa Maria - UFSM, sob o acompanhamento do professor anfitrião, Prof. Martin Wolter.
O objetivo da pesquisa é investigar os filtros morfológicos para a utilização em algoritmos de proteção de Sistemas Elétricos de Potência. Os filtros morfológicos foram implementados em MatLab e testados para detectar curtos-circuitos de alta impedância em redes de distribuição.

4.2 Atividades Realizadas:

1. Estudos sobre Morfologia Matemática para aplicação em Sistemas Elétricos de Potência;
2. Revisão bibliográfica sobre técnicas de detecção de falta de alta impedância em redes de distribuição;
3. Implementação de sistema teste incluindo modelo de falta de alta impedância. O sistema teste foi implementado no software Hypersim do simulador digital em tempo real Opal-RT. Esta atividade resultou em um artigo que foi apresentado em Congresso Internacional (em ANEXO).
4. Implementação de filtros morfológicos para fins de detecção de faltas de alta impedância. Os filtros foram implemtados no MatLab.
5. Análise da resposta dos filtros morfológicos para diferentes condições de falta de alta impedância.
6. Atividades complementares:
    - Apresentação sobre a Universidade Federal de Santa Maria e pesquisas realizadas para um grupo de professores e alunos (Anexo).
    - Aula sobre Proteção de Linhas de Transmissão para alunos de pós-graduação (Anexo).

4.3 Resultados e/ou Impactos:

1. Os filtros morfológicos podem ser usados para detectar transitórios em sistemas elétricos. No entanto, requerem um detalhado estudo para definição do melhor função do elemento estruturante.
2. Foram implementados diversos filtros morfológicos, tais como, erosão, dilatação, abertura, fechamento, diferença entre abertura e fechamento entre outros. Todos possuem capacidade de detecção de transitórios, porém os filtros diferença entre a dilatação e erosão ou diferença entre abertura e fechamento apresentam melhor desempenho para detectar as faltas de alta impedância.
3. Foram implementados dois modelos de falta de impedância no simulador digital em tempo real da Opal-RT. Um baseado em diodos anti-paralelos e outro baseado em polinômio. Os filtros morfológicos apresentaram um melhor desempenho quando foram usado o modelo de diodos em anti-pararelo.

Santa Maria , 18 de Fevereiro de 2020.

ANEXOS

- Apresentação sobre a UFSM e as atividades de pesquisa.

Visiting Professor
Research Activities
Oct – Dec / 2019

Prof. Adriano Peres de Morais, Dr. Eng.
adriano@ctism.ufsm.br
Building 9
Room 121

- Aula sobre proteção de linhas de transmissão.

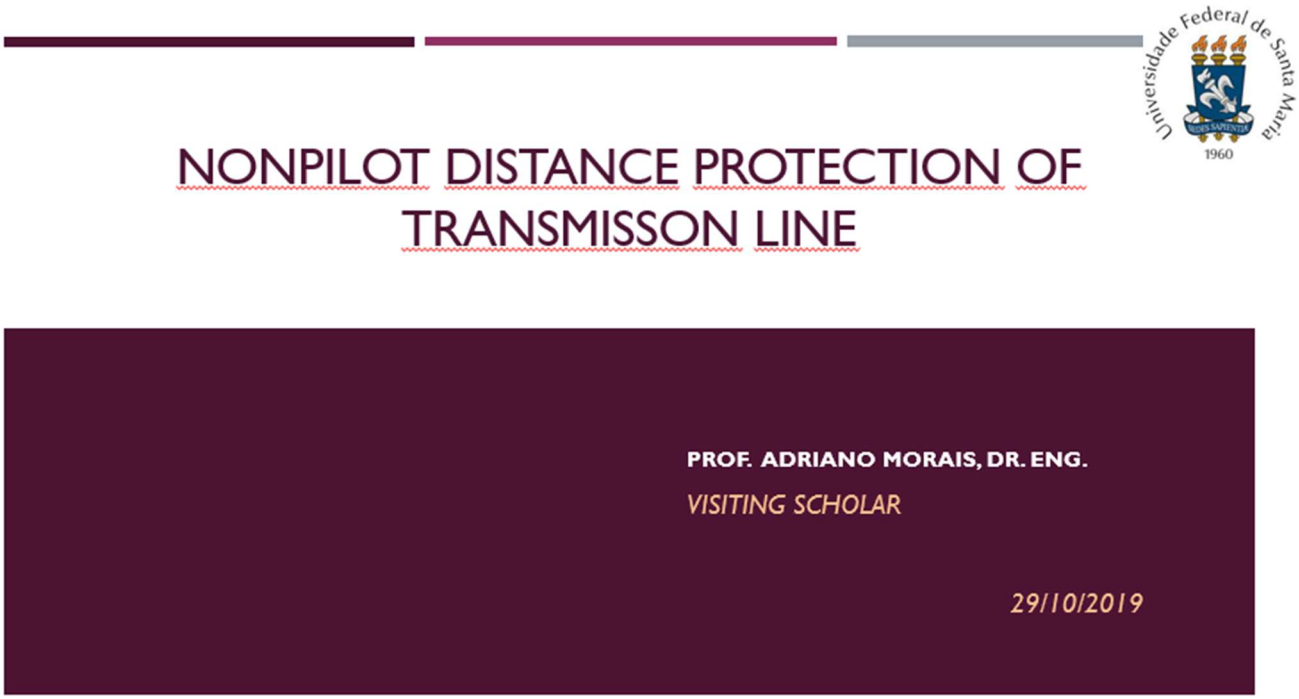

- Artigo apresentado no IECON

Validation of a Comprehensive High Impedance Fault Model for Real-Time Environment

Aldair Wontroba
Adriano Peres de Morais
Jean Pereira Rossini
Mairon Gallas
Ghendy Cardoso Junior
Federal University of Santa Maria
Santa Maria-RS, Brazil
aldair.wontroba@hotmail.com

João Paulo Abreu Vieira
Electrical Engineering Graduate Program
Federal university of Pará
Belém-PA, Brazil
jpavieira@ufpa.br

Patrick Escalante Farias
Federal Institute of Education, Science and Technology of Rio Grande do Sul - IFRS
Farroupilha, Brazil
pefarias@gmail.com

Marcelo Costa Santos
Distribution System Operation Management
CELPA –Electric Distribution Utility of Pará
Belém-PA, Brazil
marcelo.costa@celpa.com.br

***Abstract*— This paper presents a comprehensive model for a high impedance fault for real-time environment. This model offers different types of ground surface, type of high impedance fault, and it is suitable for close-loop testing relays and algorithms validations. The model is incorporated into OPAL-RT simulator and implemented in Hypersim software. Finally, the performance of the model is validated under a real case of high impedance fault by comparison with real-time simulation.**

Keywords—High impedance fault modeling, Power distribution systems, Real-time digital simulation.

I. Introduction

High Impedance Faults (HIF) are one of the most common type of fault in power electric distribution systems. HIF typically occurs when the conductors in distribution network touch the ground surface, i.e. asphalt, tree, concrete, etc. Due to the high impedance of these surfaces, the fault current generally has a low magnitude value.

Since this type of fault has a small value, classical overcurrent relays do not detect HIF. So, it is extremely rare to find oscillographic records of HIF to validate the pick-up of IEDs. Still, proposed methods for HIF detection or locations are based on not real-time simulations. Basically, commercial IEDs spend a long time installed in test mode to validate it against HIF. Proposed methods for HIF detection or even HIF location use electromagnetic softwares, such as, EMTP, to prove their efficiency. In other words, from the authors' experience there is no HIF model implemented for real-time simulation.

Hence, this paper presents a HIF flexible model for real time simulation. The model is incorporated into OPAL-RT simulator and implemented in Hypersim software. The digital model can be applied for validation of HIF detection or location algorithms (software-in-the-loop - SIL) and validation of IEDs in real-time (hardware-in-the-loop - HIL). The user can simulate HIF considering different types of ground surface, cable breakage and choose the phase in fault. The results obtained was showed and compared with a real case of HIF. The remainder of this paper is organized as follows. Section II presents the characteristics of HIF and Section III presents a literature review about HIF models. Section IV elucidates about HIF modeling for real-time simulation. The results obtained by the real-time model are presented on Section V. Section VI includes the conclusions derived from this work.

II. Characteristics of HIF

In technical terms, the IEEE PSRC [1] defines HIF as fault with current magnitude below the pick-up of the overcurrent relays. Moreover, others distinctive features can also define a HIF according to Fig. 1, such as, buildup and shoulder stages, intermittence and asymmetry of the fault current.

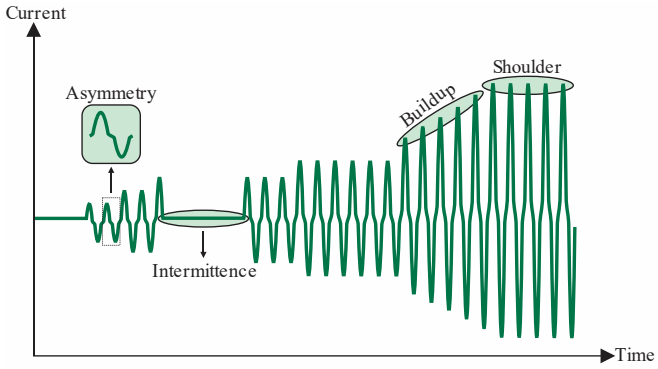

Fig. 1. Characteristics of HIF.

Buildup is the period in which the fault current increases gradually due to accommodation of the cable in the ground while the shoulder stage refers to the periods of constancy in the magnitude. Intermittence occurs when the HIF electric arc is extinct during some time due to the loss of moisture in the surface. The arc restarts when the conductor reaches another region with enough moisture to reestablish an electric path. Asymmetry is originated by the silica present in the surface that causes a great drop voltage during the negative semi cycle of the current so the positive semi cycle has a greater magnitude [2]. The asymmetry is also related to the nonlinear V x I behavior at the fault point, which is a typical HIF feature caused by the electric arc as well.

The HIF, may have three distinct configurations, as shown in Fig. 2. Shunt fault (Fig. 2.a), with no disruption of the line cable, it is usually temporary, for instance, when a tree touches the cable during a storm. On the shunt-series fault the line cable drops to the ground from the power source (Fig. 2.b) and load side (Fig. 2.c), respectively.

Fig. 2 also shows the behavior of the current, measured at substation, of a feeder during these three different types of HIF. For shunt fault, from the moment that fault occurs, it is possible to observe that the feeder current increases and the buildup and shoulder stages are apparent. For shunt-series (source side), due to cable breakage the feeder current reduces (open circuit) and after the establishment of HIF the current increases and presents a typical behavior of HIF. Finally, for the case shunt-series (load side), the current reduces and remains theoretically the same value because the source (substation) do not contributes with the fault current.

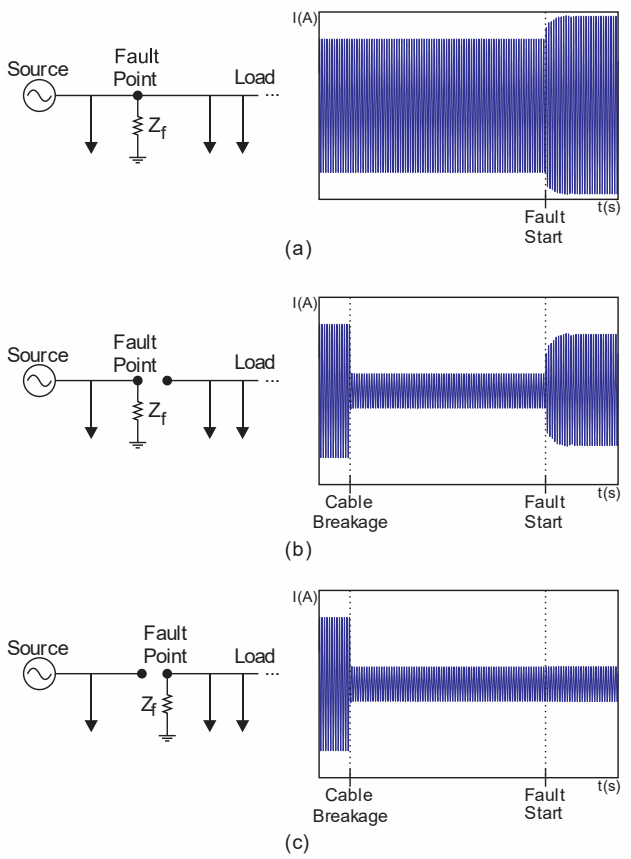

Fig. 2. Types of HIF: (a) Shunt fault (b) shunt-series fault – source side (c) shunt-series fault – load side.

III. Review of HIF Models

A correct fault model is essential for some types of power system studies, especially for HIF detection or location which most of the methodologies are based on inherent HIF features. The majority of HIF detectors uses somehow the harmonic content present in the fault current [3]-[5]; each HIF feature is responsible for a different content: low frequency (nonlinearity of V x I curve), even harmonics (asymmetry), high frequency (intermittence) and inter-harmonics (shoulder and buildup stages)[6]. Methods based on the HIF current shape are also widely applied to fault detection, which wavelet [7]-[8] and mathematical morphologic [9]-[10] methods can be highlighted due to their capability of recognize transients and distortions present in the current signal.

Basically, most published papers use one of the models presented below.

A. Model 1 [11]

This model uses a variable-impedance, connected between the fault point and the ground. The

impedance contains a fault resistance R_F, calculated according Eq.(1), and a fault inductance L_F, which has a typical value of 3mH.

$$R_F = R_{F0}\left(1 + \alpha\left(\frac{i_F}{i_{F0}}\right)^{\beta}\right) \quad (1)$$

Where:
R_{Fo} is the initial fault resistance;
α is a coefficient defined by the user;
β is coefficient defined by the user;
I_F is the fault current;
I_{Fo} is the initial fault current.

Despite the fact that this model is very simple to implement, it has some variables defined empirically. It makes the model not suitable for real-time validation, i.e. it is difficult compare a simulation with a real case of HIF.

B. Model 2 [12]

This model uses two diodes and two DC voltage sources, connected in antiparallel. Between the source and the diodes are connected a resistance RF and a inductance LF, as show Fig. 3. When the voltage of the AC source is greater than the voltage Vp, the short-circuit current will flow from the source to ground. The current will have the opposite direction when the AC voltage is less than Vn. If the AC voltage is between Vp and Vn, AC is counterbalanced by Vp or Vn in such a way that no fault current would flow.
This model is not practical if the user intends to consider different types of ground surface. Besides, it does not consider the buidup stage.

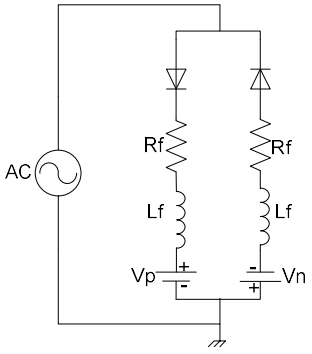

Fig. 3. Model of HIF using two antiparallel diodes.

C. Model 3 [13]

The model proposed in [13] consists of two variable resistances in series. The first one (R_1) models the growing feature of the current during the settling time of the conductor in the soil (buildup stage). The second one (R_2), models the typical asymmetry of the electric arc and is present in all fault current cycles. Fig. 4 represents the model of variable resistance.

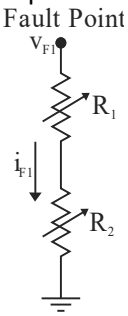

Fig. 4. Model of variable resistance.

In consequence, the voltage at the fault point (v_F) is given by (1).

$$v_F(t) = v_{R1}(t) + v_{R2}(t) \quad (1)$$

Where: $v_F(t)$ is the instantaneous voltage at the fault point; $v_{R1}(t)$ and $v_{R2}(t)$ are the instantaneous voltage on the resistors R_1 and R_2, respectively.

1) R_1 Control

The R_1 resistance emulates the buildup period, that is, the growth characteristic of the fault current during the period of accommodation of the cable in the ground. For this, R_1 has a high value in the beginning of the fault and decreases its value gradually over time to a value close to zero. To represent this behavior, [2] proposed the use of a polynomial according to (2). The order of this polynomial, as well as its coefficients, depends on the type of soil in which the HIF occurred.

$$R_1(t) = \begin{cases} c_k.t^k + c_{k-1}.t^{k-1} + \ldots + c_1.t + c_0, & se\ t < \Delta t \\ 10^{-5}, & se\ t \geq \Delta t \end{cases} \quad (2)$$

Where: k is the degree of the polynomial and index of each coefficient; c are the coefficients of the polynomial; Δt is the period of growth of the fault current.

2) R_2 Control

The second resistance (R_2) models the asymmetric characteristic of the V x I curve due to the presence of the electric arc and is present in all cycles of the fault current. For this, a routine checks if the voltage at the fault point is in the increasing branch (positive derivative) or decreasing (negative derivative) of the V x I curve of the surface in which the HIF will be simulated. After verifying the branch, the routine uses (3) to obtain the respective fault current of the V x I curve. Finally, the corresponding resistance is calculated through the OHM Law.

$$i_F(t) = \begin{cases} i_{Fi}(m) + \dfrac{i_{Fi}(m+1) - i_{Fi}(m)}{v_{Fi}(m+1) - v_{Fi}(m)} . \Delta v, \\ \text{if } v_{Fi}(m) < v_F(t) < v_{Fi}(m+1) \\ i_{Fi}(m), \\ \text{if } v_F(t) = v_{Fi}(m) \end{cases} \quad (3)$$

Where: $v_F(t)$ is the voltage at the fault point; $\Delta v = v_F(t) - v_{Fi}(m)$; $v_{Fi}(m)$ and $i_{Fi}(m)$ are the voltage; the current of the characteristic curve V x I in sample m, respectively. In the first version of the model proposed by [13], R_2 was calculated only with the data of the V x I curve for a stone surface. However, in the modification proposed by [2], the model became more complete, adding the V x I curves of six other surfaces according to Fig. 5.

IV. HIF Modeling for Real-Tiime Simulation

For the reason discussed in section V, the HIF model proposed by [13] has been chose. The HIF model was implemented and simulated with Opal-RT real time simulator and Hypersim software. Opal-RT/Hypersim simulator performs real-time simulations and non-real-time simulations. In this work all the tests were performed in real-time mode. To be considered real-time the simulation, the runtime, T_e, must be less than or equal to the selected time, as shown Fig. 6.a, and case, T_e is greater than its time-step size for one or more time-steps, overruns occurs and the simulation is considered as non-real-time, as shown Fig. 6**Erro! Fonte de referência não encontrada.**.b. This can

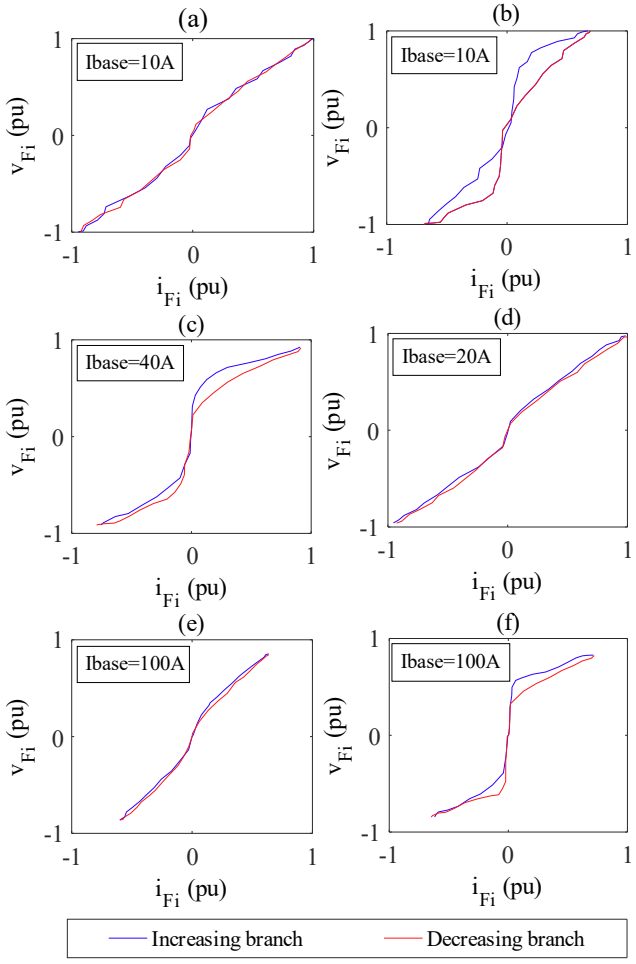

Fig. 5. V x I Curves at the HIF point corresponding to one cycle: a) sand, b) asphalt, c) gravel, d) cobblestones, e) grass, f) local soil.

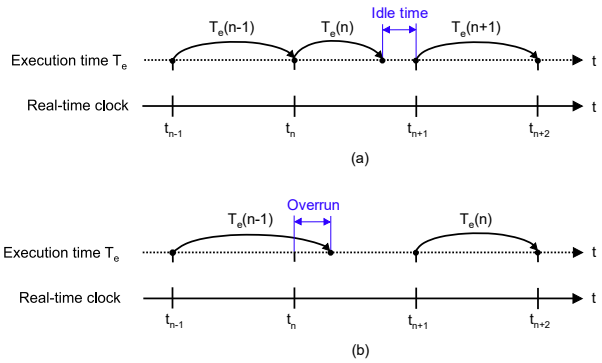

Fig. 6. Illustration of real-time and offline simulation. (a) Real-time simulation. (b) Non-real-time simulation.

sometimes lead to a tradeoff between model-detail and ability for real-time implementation. It means that a detailed model requires more computation time per time step.

In this work the test system was implemented within the graphic interface of Hypersim, and the HIF model was implemented in a UCM block (User Code Model), which not only have control interface but also

is equipped with electrical interfaces. The UCM is a Hypersim utility that permits users to build their specific blocks in the model using a C-coded function while respecting the Hypersim programming rules.

A UCM is composed of a power part and a control part:

The power part has external nodes (graphically visible) and internal nodes (invisible). An advantage of using the UCM is that its power part is solved simultaneously with other power components. Because the UCM's power part is solved together with other power elements, user must follow the same procedure used in Hypersim algorithm to solve node voltages. The control part is simply a relationship between inputs and outputs and is simpler to model. Fig. 7, the UCM blocks used for HIF model can be visualized as well as the test system used for model testing.

The six ground surfaces present in [13] are implemented in the model using the resistors R_1 and R_2 as mentioned on subsection III.C.

In order to better validate the model, another case of HIF was implemented based on a real occurrence of HIF. To model such a case, the current and voltage at the fault point were estimated and then the V x I curve was obtained for R_1. Resistor R_2 was neglected since there is no record of buildup in the extracted oscillographs. In this case the estimation of the voltage and current at the fault point was only possible due to HIF occurring very close to the substation and also the breakage of the cable was verified. In this way, the voltage and currents measured at the substation can be considered as values at the point of failure.

Fig. 8 shows the HIF mask using UCM block. The user can simulate up to 6 different types of ground surfaces and one real case. Each one is identified using a pre-defined number as shown TABLE I. Besides, the user can select the phase which the fault will be applied and if there is line cable breakage or no as well as the time between the break and the fault.

TABLE I. Type of ground surface and identification number.

	Type of ground surface						
Surface	Sand	Asphalt	Gravel	Cobbl.	Grass	Local Soil	Real Case
N°	0	1	2	3	4	5	6

v. Results

The test system implemented is presented in Fig. 7. The parameter of test system was obtained from the real Brazilian feeder, which belongs to CELPA utility (*Centrais Elétricas do Pará*). The ideal source is 69 kV, the parameters of the the lines, transformer and the feeder section (substation to fault point) are presented in the TABLE II. The load is connected in delta. The HIF insertion occurs in BUS_HIF in only one phase. The tests were carried out using three digital to analog outputs of the OPAL-RT. The transformer relation is 69/13.8 kV and delta-grounded wye connection. The values of the table are in *p.u.* on a basis of 100MVA. The experimental setup is shown in Fig. 9.

TABLE II. Impedance of the test system elements.

	Positive sequence		Zero sequence	
	R	X	R	X
Line 1	0.0155	0.0366	0.045	0.1449
Line 2	0.0127	0.03	0.037	0.1189
Transformer	0	0.507	0	0.507
Feeder	0.0158	0.0205	0.0274	0.1465

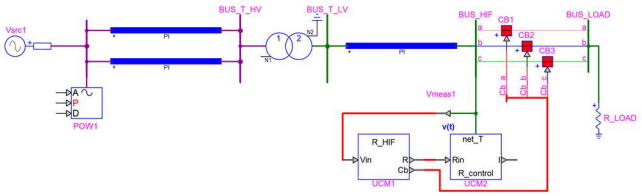

Fig. 7. Test system.

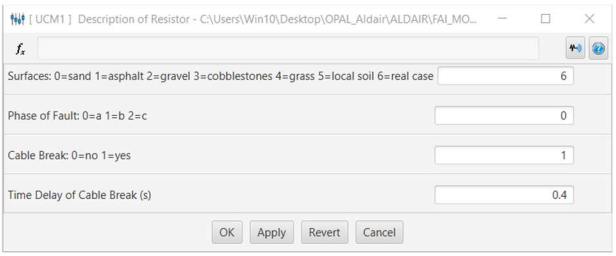

Fig. 8. HIF user mask.

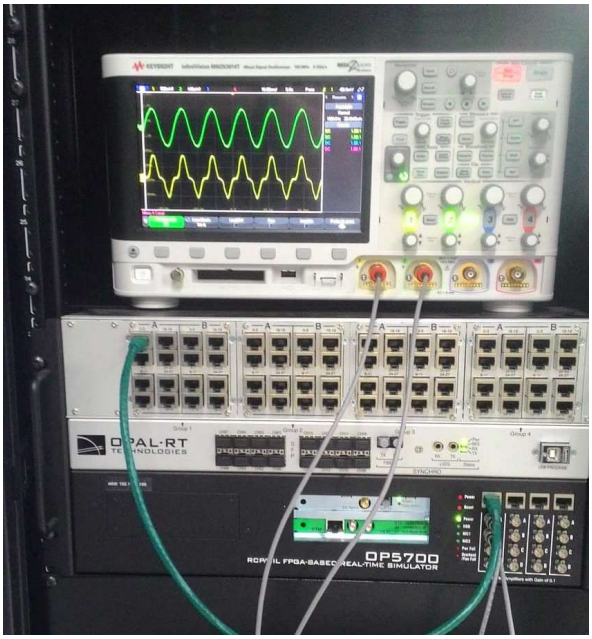

Fig. 9. Experimental setup using OPAL-RT for real-time simulation of HIF model.

A. Time step evaluation

The performance of the HIF model has been evaluated for three-time steps. Fig. 10 presents the response of the model for the three different time steps, i.e. 500µs (a), 100µs (b) and 10µs (c). The simulations have considered a ground surface based on cobblestone (case 3). It is possible to observe that the representation of HIF current loses accuracy for 500µs, but for 100µs it is possible to represent the characteristics of the HIF with a good precision. The low accuracy may cause a bad representation for harmonics evaluation and distort test of HIF detection algorithm.

The time-step can be change depending on the system simulated. For this test system and HIF model simulations, the OPAL-RT executed in approximated 0.75µs each time-step using just one core. However, it can change during simulation if the system has non-linear elements and interactive mode was able. All results presented in the next figures were carried out with 50µs of time-step and captured from an oscilloscope.

B. Cable breakage

The HIF model allows the user simulate faults with disruption of the line cable or without disruption of the cable. Fig. 11.a shows the current, measured at substation, with no cable breakage and Fig. 11.b considering a cable breakage. The time between cable breakage and fault can be chose by the user. In Fig. 11.b this time is defined as 300ms.

The ground surface of Fig. 11 is the case 2, i.e. gravel surface. It is possible to see that buildup and shoulder are present clearly and is similar with the results obtained for [2].

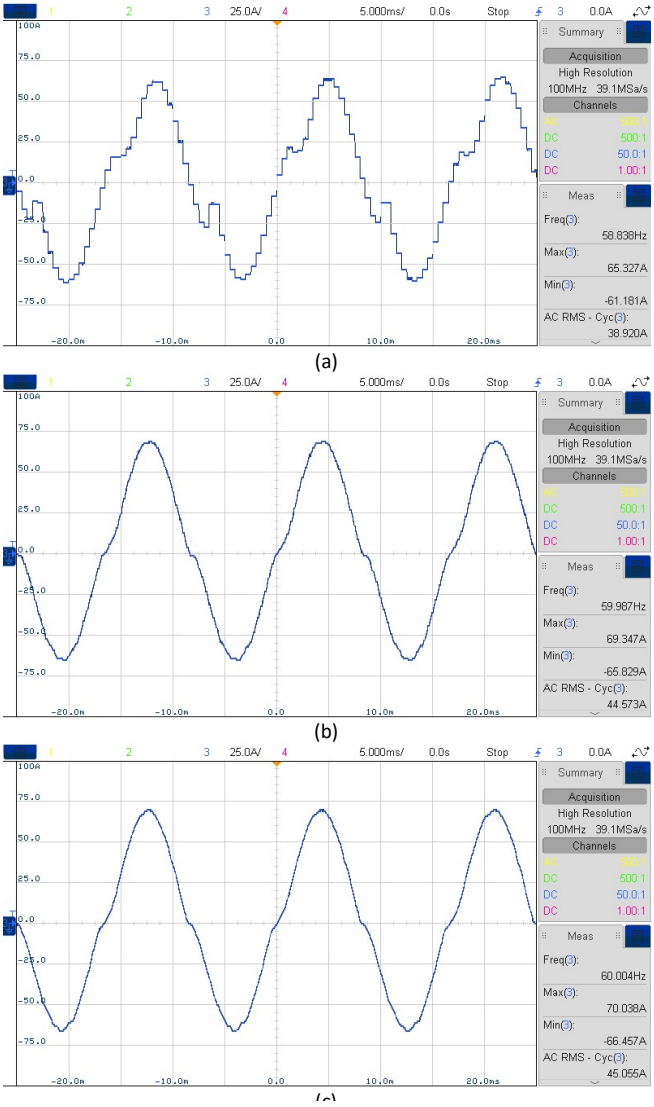

Fig. 10. Performance of the HIF model for three time-steps, (a) 500µs, (b) 100µs, (c) 10µs.

C. Ground surface simulations

The model implemented in Hypersim can support 6 types of ground surfaces and one real case, based on oscilografy. Fig. 12 and Fig. 13 show the current of the HIF at point of fault for different views. Three types of soil were simulated (a) sand, (b) cobblestones and (c) local soil. In the Fig. 12 it is possible to observe the

buildup and shoulder stage. The asymmetry and distortion of current can be seen in a zoom view (Fig. 13).

D. Real case representation.

The digital HIF model has been also validated for a real case of HIF. This fault has occurred in a feeder of CELPA and the conventional overcurrent protection has not detected this case, as expected. Fig. 14 shows the current, measured at main substation, for a real case of HIF based on oscilografy and its Hypersim simulation.

The buildup and shoulder periods were neglected, because they are not present in the oscilografy data. However, it is possible to observe the similarity of the current amplitudes and the asymmetry of the waveform in the phase in fault due to the electric arc.

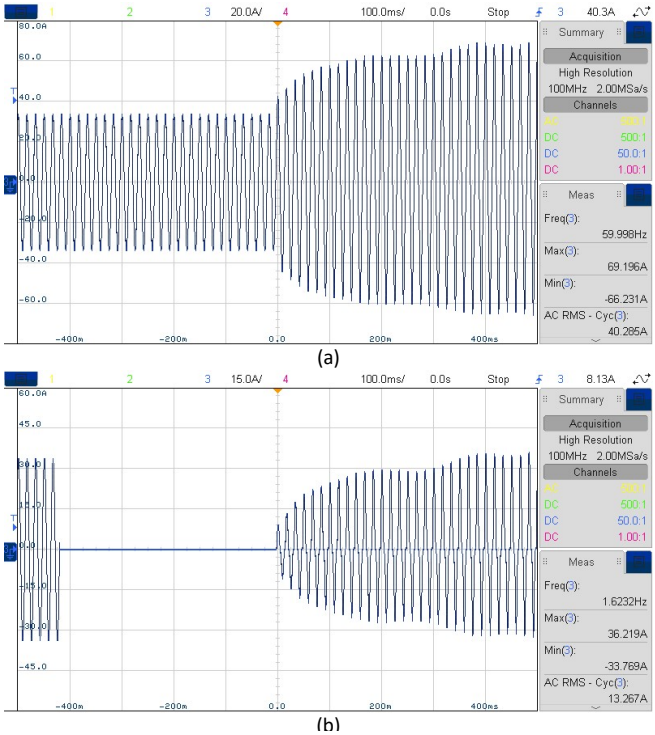

Fig. 11. (a) current with no cable break and (b) with cable break.

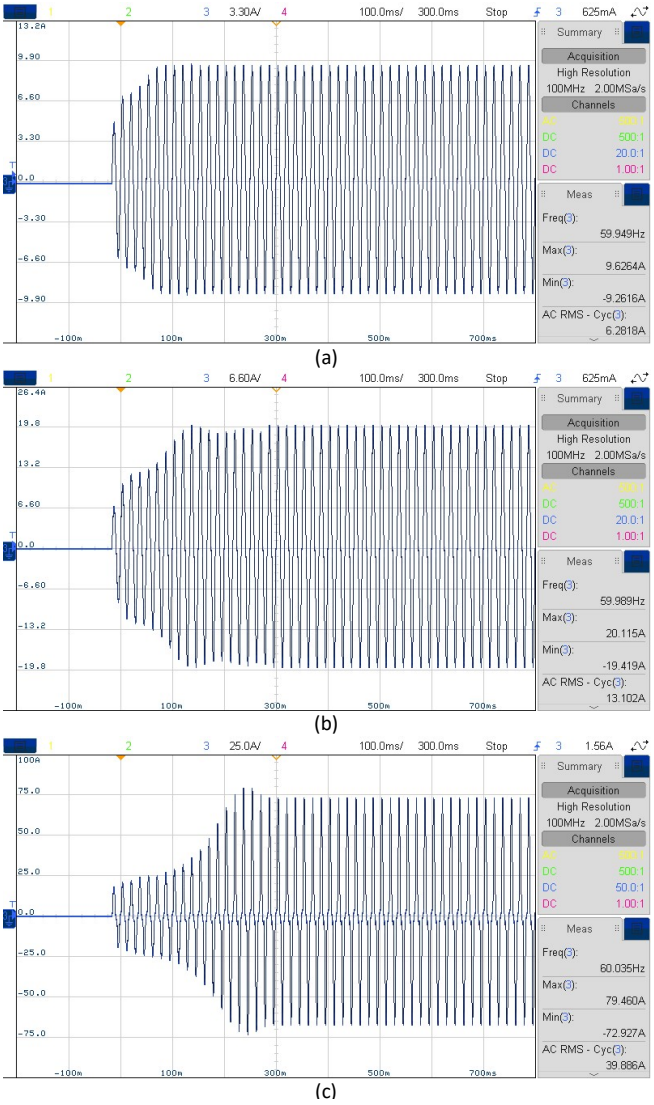

Fig. 12. Current at fault point of (a) 0-sand, (b) 3-cobblestones and (c) 5-local soil.

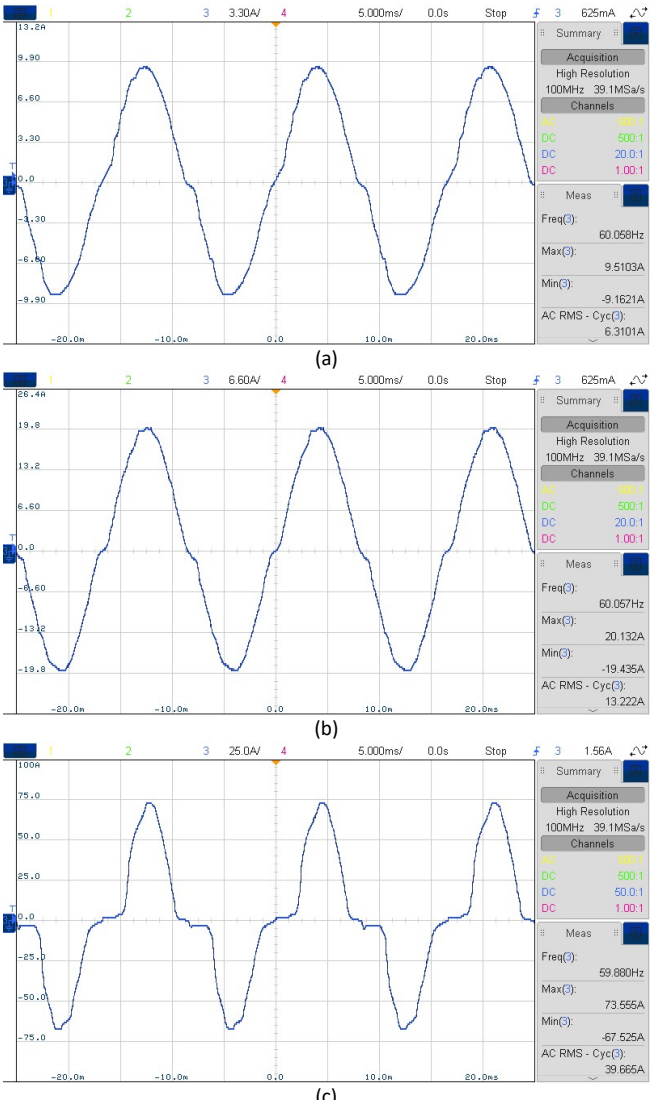

Fig. 13. Current at fault point of (a) 0-sand, (b) 3-cobblestones and (c) 5-local soil.

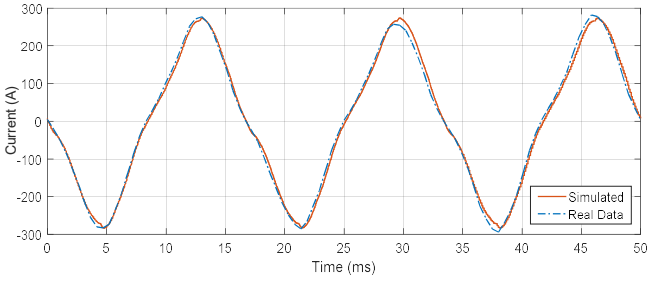

Fig. 14. Real data vs Simulated.

VI. CONCLUSIONS

A comprehensive HIF model for real-time application has been developed in Opal-RT simulator. Implementation aspects, such as, time step, were discussed. This method allows representation of all the HIF characteristics as buildup stage, shoulder stage and asymmetry of the electric arc. Furthermore, the presented model considers six types of soil, a real case of HIF. The HIF model also considers important details, such as, cable brekage and phase of fault.

The simulation results illustrate the behavior of the fault current is very similar to a real case of HIF. The next step of this research is to apply this model to test HIF IEDs .

Acknowledgment

The authors are grateful to CELPA for the financial support in developing this work, which is part of a R&D project.

This study was financed in part by the *Coordenação de Aperfeiçoamento de Pessoal de Nível Superior - Brasil (CAPES/PROEX) - Finance Code 001* and *Conselho Nacional de Desenvolvimento Científico e Tecnológico – CNPq*.

References

[1] J. Tengdin, et al.; “High Impedance Fault Detection Technology”, *Report of PSRC Working Group D15*, March 1996.

[2] W. C. dos Santos, B. A. de Souza, N. S. D. Brito, F. B. Costa and M. R. C. Paes Jr., “High Impedance Faults: From Field Tests to Modeling”, *Journal of Control, Automation and Electrical Systems*, pp. 885-896, September 2013.

[3] S. M. Shahrtash, M. Sarlak, “High impedance fault detection using harmonics energy decision tree algorithm”, *International Conference on Power System Technology*, pp. 1–5, 2006.

[4] H. G. Yeh, D. H. Tran, R. Yinger. “High impedance fault detection using orthogonal transforms”, *IEEE Green Energy and Systems Conference*, November 2014.

[5] S. R. Samantaray, P. K. Dash, S. K. Upadhhyay, “Adaptive Kalman Filter and Neural Network Based High Impedance Fault Detection in Power Distribution Networks”, *International Conference on Power System Technology*, October 2006.

[6] E. M. Lima, C. M. S. Junqueira, N. S. D. Brito, B. A. de Souza, R. A. Coelho, H. G. M. S. de Medeiros, “High impedance fault detection method based on the short-time fourier transform”, *IET Generation, Transmission & Distribution*, vol. 12, pp. 2577-2584, June 2018.

[7] I. Baqui, I. Zamora, J. Mazn, G. Buigues, “High impedace fault detection methodology using wavelet transform and artificial neural networks”, *Electric Power Systems Research*, vol. 81, pp. 1325-1333, July 2011.

[8] F. B. Costa, B. Souza, N. Brito, J. Silva, W. Santos, “Real-time detection of transients induced by high-impedance faults based on the boundary wavelet transform”, *IEEE Transactions on Industry Applications*, v. 51, pp. 5312-5323, May 2015.

[9] S. Gautam and S. M. Brahma, “Detection of High Impedance Fault in Power Distribution Systems Using Mathematical Morphology”, *IEEE Transactions on Power Systems*, vol. 28, no. 2, pp. 1226-1234, May 2013.

[10] M. Sarlak and S. Shahrtash, “High-impedance faulted branch identification using magnetic-field signature analysis”, *IEEE Transactions on Power Delivery*, vol. 28, January 2013.

[11] A. M. Sharaf, S. I. Abu-Azab, “A smart relaying scheme for high impedance faults in distribution and utilization networks”, 2000 Canadian Conference on Electrical and Computer Engineering. Conference Proceedings. Navigating to a New Era (Cat. No.00TH8492), May 2000.

[12] A. E. Emanuel, D. Cyganski, J. A. Orr, E. M. Gulachenski,“High impedance fault arcing on sandy soil in 15 kV distribution feeders:

contributions to the evaluation of the low frequency spectrum", *IEEE Transactions on Power Delivery*, v. 5, n. 2, p. 676–686, Abril 1990.

[13] S. R. NAN, J. K. Park, Y. C. Kang, T. H. Kim, "A modeling method of a high impedance fault in a distribution system using two series time-varying resistances in EMTP",*Summer Meeting 2001: IEEE Pres*, v. 2, p. 1175–1180, 2001.

[14] A. Avendaño, "Testing the High-Impedance Fault Detector Element in the SEL-751 and SEL-451", SEL Application Guide, vol. 3, 2015.

[15] S.R. Nan, J. K. Park, Y. C. Kang and T. H. Kim, "A modeling method of a high impedance fault in a distribution system using two series time-varying resistances in EMTP", *Power Engineering Society Summer Meeting*, pp. 1175–1180, July 2001.

[16] A. E. Emanuel, D. Cyganski, J. A. Orr, S. Shiller, E. M. Gulachenski, "High impedance fault arcing on sandy soil in 15 kV distribution feeders: contributions to the evaluation of the low frequency spectrum", IEEE Transactions on Power Delivery, vol. 5, pp. 676-686, April 1990.

[17] P. M. Menghal and A. J. Laxmi, ''Real time simulation: Recent progress & challenges,'' in Proc. Int. Conf. Power, Signals, Controls Comput. (EPSCICON), Thrissur, India, Jan. 2012, pp. 1–6.

[18] T. Berry, A. R. Daniels, and R. W. Dunn, ''Real time simulation of power system transient behaviour,'' in Proc. 3rd Int. Conf. Power Syst. Monitor. Control, London, U.K., Jun. 1991, pp. 122–127.

[19] P. E. Farias, "Método para estimação da distância de faltas de alta impedância em redes de distribuição de energia elétrica considerando diferentes tipos de solo", Universidade Federal de Santa Maria, 2017.